Centerline Cracking in Deep Penetration Electron Beam Welds in Type 304L Stainless Steel

A localized shift in solidification behavior along the weld centerline promotes hot cracking

BY J. C. LIPPOLD

ABSTRACT. Two combinations of deep penetration, autogenous electron beam welds in Type 304L stainless steel exhibit a significant variation in hot cracking susceptibility which can be associated with the solidification behavior along the weld centerline. In one combination, the entire fusion zone solidifies as primary ferrite and is immune to cracking. In the other combination, a localized shift in solidification from primary ferrite to primary austenite along the weld centerline results in hot cracking within the fully austenitic region.

The shift in solidification behavior is not associated with any detectable segregation of major alloying elements but appears to be related to an abrupt change in solidification conditions at the centerline. A model is proposed which describes the effect of the weld pool shape on the local solidification growth rate and resultant solidification mode in high velocity welds in 300-series stainless steels.

Introduction

The electron beam (EB) welding process is ideally suited for producing deep penetration welds in applications where it is desirable to both minimize the weld heat input and reduce the weld-induced distortion of the component. Unfortunately, when the depth-to-width ratio of the weld is relatively high (on the order of 5 or greater), the weld is often susceptible to cracking along the centerline of the fusion zone.

Changes in the weld joint geometry and the process parameters are often helpful in reducing or temporarily eliminating the cracking. However, a permanent solution to the problem is generally not obtained until the underlying metallurgical phenomenon is understood. This investigation documents the incidence of centerline cracking in deep penetration EB welds between Type 304L stainless steel forgings and describes the mechanism responsible for cracking in these welds.

Weld Cracking Susceptibility of Type 304L Stainless Steel

Numerous investigators (Refs. 1-13) have studied the relationship among composition, weld ferrite content, and the hot cracking susceptibility of the 300-series stainless steels. The earliest studies (Refs. 1-3) recognized that the resistance of these alloys to weld hot cracking was related to the delta ferrite content of the as-deposited weld; weld deposits which contained at least 5 volume-percent (vol-%) ferrite were relatively immune to hot cracking.

More recently, Masumoto *et al.* (Ref. 5) postulated that solidification behavior, not the absolute ferrite content, was the factor which dictated whether crack-free welds could be produced. Alloys, which solidified with delta ferrite as the primary solidification product, were more resistant to cracking than alloys of similar composition which solidified with austenite as the primary phase, irrespective of the ferrite content of the as-welded microstructure.

The presence of over 5 vol-% delta ferrite in the fusion zone of Type 304L stainless steel welds generally indicates that solidification has occurred as delta ferrite. Below approximately 2 vol-%, weld solidification occurs as austenite with a corresponding increase in the weld cracking susceptibility (Refs. 6-8). Thus, in a broad sense, the ferrite content of the weld can be used to predict the relative cracking resistance of the weld metal.

A great deal of effort has focussed on predicting the eventual weld ferrite content based on the composition of the base material. Diagrams have been devised by Schaeffler (Ref. 14), Hull (Ref. 15), and DeLong (Ref. 16) which estimate the ferrite content as a function of the ratio of ferrite-forming elements to austenite forming elements. More recently, these elemental relationships have been modified by Suutala (Ref. 17) and Hammar and Svenson (Ref. 18). The DeLong diagram was the first of these equivalency relationships to include the effect of nitrogen as an austenitizing element; as a result, this diagram has become the most widely used method for predicting ferrite content.

The DeLong diagram, with the chemical composition limits of Type 304L stainless steel superimposed, is shown in Fig. 1. A large area in the upper lefthand

J. C. LIPPOLD is with Sandia National Laboratories, Livermore, California.

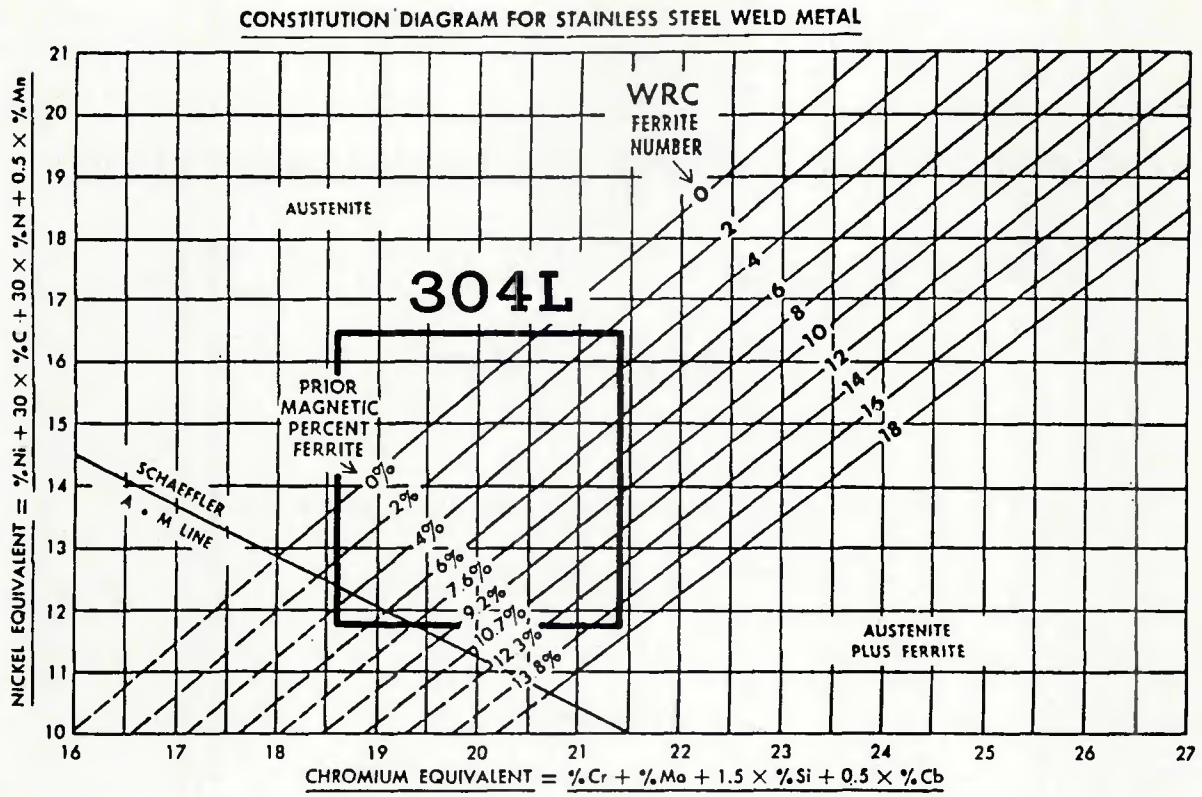

Fig. 1—Composition limits of Type 304L stainless steel superimposed on the DeLong diagram

portion of the enclosed region corresponds to Type 304L stainless steel compositions relatively rich in austenite-forming elements (Ni, Mn, C, N) and depleted in ferrite-forming elements (Cr, Si, Mo) which would exhibit little or no ferrite in the as-welded microstructure. Since the initial solidification product of alloys in this region would most likely be austenite, their resistance to hot cracking would be inferior to alloy compositions located in the lower righthand portion of the enclosed region. Thus, when formulating or selecting heats of Type 304L stainless steel which will be immune to weld hot cracking, it is necessary to restrict the compositions to those which will produce a sufficient amount of weld metal ferrite (greater than 2 vol-%).

Solidification Behavior

The primary phase of solidification in Type 304L stainless steel welds is predominantly a function of the weld metal composition. In addition, the composition has a strong influence on both the weld ferrite content and the ferrite morphology. When solidification occurs as austenite, chromium partitions to the last-to-solidify regions at the cellular or dendritic boundaries and promotes the formation of ferrite at these locations. Ferrite formation during the final stages of solidification is generally considered to be the result of a eutectic reaction (Refs. 5,12,13,19,20). The delta ferrite remaining in the room temperature microstructure is generally associated with the solidification substructure boundaries.

An increase in the weld ferrite content above 2-3 vol-% in Type 304L stainless steel is usually accompanied by a shift to solidification as primary ferrite. During solidification as ferrite, austenite-forming elements (primarily nickel) partition to the solidification substructure boundaries and promote the formation of austenite during the final stages of solidification. Upon further cooling in the solid state, a large fraction of the primary ferrite transforms to austenite, thus reducing the room temperature ferrite content to the levels predicted by the DeLong diagram—Fig. 1. The mechanics of both primary ferrite solidification (Refs. 19,21-25) and the solid state ferrite-to-austenite transformation (Refs. 22, 23, 26, 27) have been the subject of extensive research in the past decade; the references cited above will provide the reader with details of each of these metallurgical phenomena.

The ferrite morphology resulting from the incomplete ferrite-to-austenite transformation may vary greatly within the allowable limits of the Type 304L stainless steel composition. Under normal welding conditions (moderate weld heat input and welding speed), the ferrite morphology in welds of Ferrite Number (FN) 3-8 is discontinuous and has been described as both vermicular (Ref. 19) and skeletal (Ref. 26).

As the weld FN increases above FN 8, ferrite begins to form a continuous network within the microstructure. With a further increase in the weld FN, the ferrite takes on an acicular, or lathy, appearance (Ref. 28). In Type 304L stainless steel weldments, the transition from the skeletal to the acicular ferrite morphology occurs somewhere in the range of FN 10-15. Since the composition of Type 304L stainless steel is biased toward lower ferrite contents (Fig. 1), the acicular morphology is only occasionally observed.

Effect of Welding Process Conditions

The majority of the studies concerned with solidification behavior and transformations in austenitic stainless welds have concentrated on weld microstructures which are produced using the more conventional welding processes (*e.g.*, SMAW, GTAW, GMAW). Within a fairly broad range of weld process conditions, the weld ferrite content and, to a lesser extent, the ferrite morphology are relatively constant and appear to be almost entirely dependent on the weld metal composition. Suutala (Ref. 17) has shown, however, that as the weld travel speed is progressively increased during GTA welding of thin sheet, solidification as primary austenite is favored. The reduction in weld ferrite content associated

Table 1—Chemical Compositions of the Type 304L Stainless Steels

Material	Cr	Ni	Mn	Si	N	C	P	S	Calculated equivalents[a] Cr	Calculated equivalents[a] Ni
A	18.6	11.8	1.73	0.43	0.054	0.033	0.04	0.016	19.3	15.3
B	18.8	10.4	1.68	0.65	0.039	0.024	0.04	0.004	19.8	13.1
C	18.3	10.4	1.51	0.56	0.025	0.020	0.04	0.007	19.1	12.5
Composition Limits	18.0 / 20.0	10.0 / 12.0	1.50 / 2.00	0.30 / 0.70	0.020 / 0.080	0.015 / 0.030	0 / 0.04	0 / 0.015		

[a]Calculated using DeLong equivalents

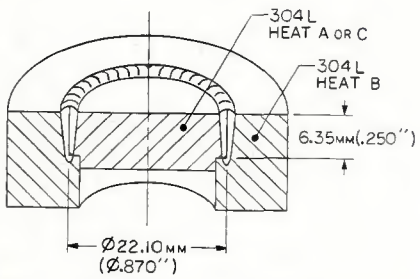

Fig. 2—Schematic illustration of the weld joint geometry

with this gradual shift in solidification behavior is usually small and, as a result, is not indicative of a change in the primary phase of solidification.

A more dramatic reduction in the weld ferrite content was observed by Vitek and David (Ref. 29) in laser welds produced in Type 308 and Type 312 austenitic stainless steels. For example, high speed laser welds made on a Type 308 stainless steel weld surfacing deposit, which initially solidified as primary ferrite, exhibited approximately FN 1 and appeared to solidify as primary austenite. The ferrite, which formed in these welds, was extremely fine and was situated along the solidification subgrain boundaries. The shift in solidification behavior did not reduce the hot cracking resistance of the material.

The results of Vitek and David indicate that the use of high energy density, low heat input welding processes such as laser and electron beam welding may severely alter the amount and morphology of the delta ferrite, which is normally expected in the austenitic stainless steels. Perhaps more important, however, is the shift in solidification mode, which is concomitant with the reduction in ferrite. This investigation will describe similar shifts in solidification behavior which occur in electron beam welds in Type 304L stainless steel and relate this shift to the cracking susceptibility of these welds.

Materials and Experimental Approach

Materials

The chemical composition and related chromium and nickel equivalents of the three heats of Type 304L stainless steel used in this investigation are listed in Table 1. Two of the materials (A and C) were in the form of circular forgings produced from 31.8 mm (1.25 in.) thick cross-rolled plate. These forgings were subsequently machined into 22 mm (0.87 in.) diameter circular plugs. Material B was forged from 51 mm (2.0 in.) diameter bar stock and subsequently machined into a ring-shaped geometry with an inner diameter which matched the dimensions of the circular plugs. The minimum allowable yield strength of the forgings was 310 MPa (45 ksi).

Table 2—Electron Beam Welding Conditions

Accelerating voltage	125 + 2 kV
Beam current	12.0 + 0.5 mA
Travel speed	8.47 mm/s (20 ipm)
Focus setting	Sharp
Electron beam gun-work distance	15.24 cm (6 in.)
Part rotation	440-460 degrees
Part fit/gap	0.025-0.125 mm (0.001-0.005 in.)

Welding Procedure

A schematic illustration of the plug weld sample is shown in Fig. 2. A single pass, autogenous electron beam weld was used to join the two parts. Welds were made with two material combinations, namely A/B and B/C. Acceptance criteria required weld penetration to exceed 6.3 mm (0.25 in.).

All welds were performed with the conditions listed in Table 2. Actual welding required somewhat more than one full revolution in order to accommodate the slope-up and slope-down to full power. Following welding, ultrasonic inspection techniques were employed to detect the presence of any weld defects which may be present above the 6.3 mm (0.25 in.) step. The ultrasonic technique was sensitive to any lack-of-fusion defects, porosity, or weld cracks which exceeded approximately 0.25 mm (0.01 in.) in the largest dimension. Weld crack locations were indexed in order that transverse cross sections could be removed for metallographic examination.

Analytical Procedures

Transverse metallographic sections were removed at 90 deg locations referenced to the slope-up/slope-down position of the weld. In addition, welds containing crack-like indications were sectioned to reveal these discontinuites. The samples were metallographically polished through 0.05 micron* alumina and subsequently etched with either a mixed acid (equal parts acetic, nitric, and hydrochloric) or a 10% oxalic acid solution (electrolytic).

Weld sections containing large centerline cracks were carefully sectioned so as to expose the crack surface. A scanning electron microscope (SEM) equipped with an energy dispersive spectrometer was used to characterize the fracture morphology and identify particles and/or features associated with fracture surface. In addition, the electron microprobe was utilized to obtain compositional profiles from pertinent regions of the weld microstructure.

Results

Predicted Solidification Behavior

The ferrite content, or ferrite number (FN), of electron beam welds between material combinations A/B and B/C can be predicted on the basis of the average weld metal composition using the DeLong diagram in Fig. 1. In addition, the demarcation between solidification as primary ferrite and primary austenite, which has been proposed by Suutala *et al.* (Refs. 20,22), can be superimposed on this same diagram, as shown in Fig. 3. Alloys which lie above this line would be expected to solidify as austenite, while below the line the primary solidification product should be ferrite.

The electron beam welds in this investigation were made with the beam centered on the weld interface between the two materials. Thus, it is reasonable to assume that equal mixing of the materials

**1 micron = 0.00004 in.*

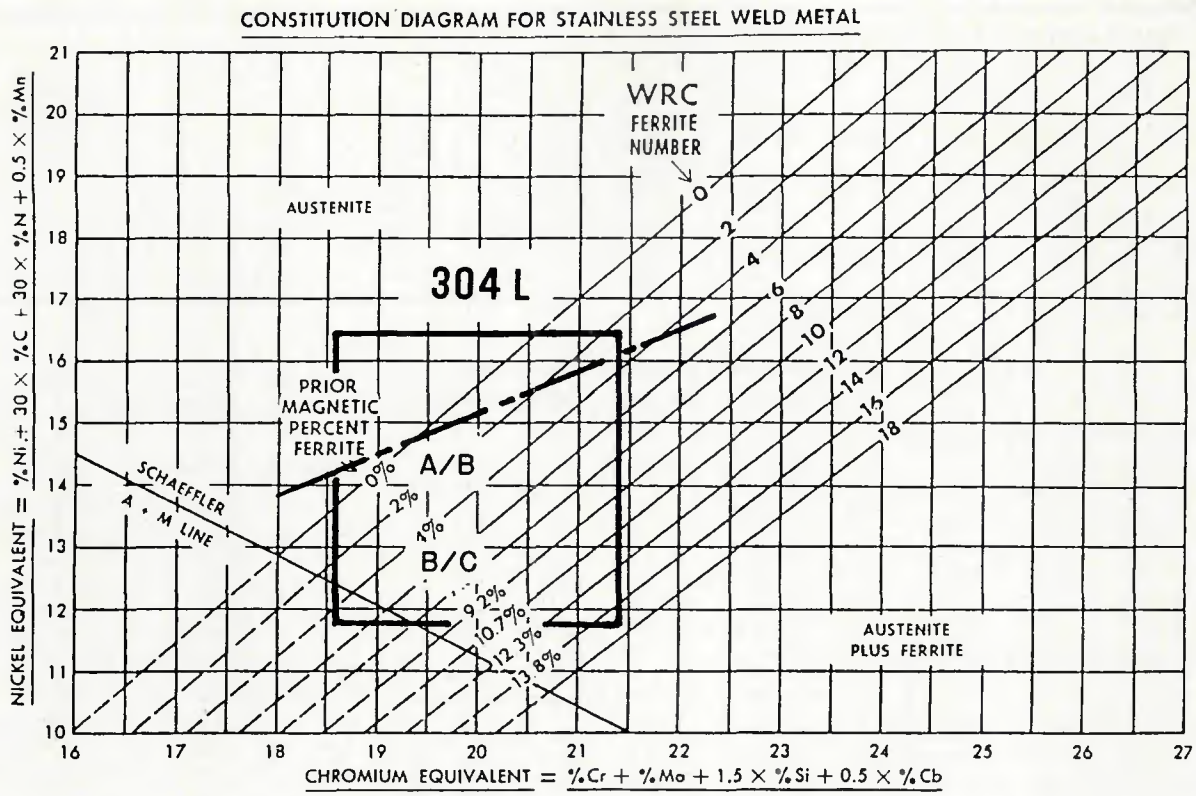

Fig. 3—The DeLong diagram with the Suutala demarcation superimposed

occurs in the weld pool. Weld metal compositions representative of this equal mixture in both the A/B and B/C welds have been plotted on the diagram in Fig. 3. The diagram predicts that both of the EB weld compositions should solidify as primary ferrite, although the A/B composition lies closer to the demarcation line and would predict a lower weld ferrite content than the B/C welds.

Weld Microstructures

B/C welds. A macrograph of a transverse section of a representative B/C electron beam weld is shown in Fig. 4. The weld has penetrated past the step located 6.35 mm (0.25 in.) below the top of the sample (see Fig. 2) and exhibits a depth-to-width ratio of approximately 9. The dark-etching appearance of the weld indicates the presence of delta ferrite in the as-welded microstructure.

The ferrite content of the weld, as measured by the Magne Gage, was nearly FN 5 and thus closely approximates the ferrite level predicted by the DeLong diagram—Fig. 3. The ferrite distribution within the weld was relatively uniform with the exception of a fully austenitic region at the root of the weld. The ferrite morphology in the B/C welds was typically of the vermicular (skeletal) type. The combination of ferrite content and morphology in these welds suggests that solidification has occurred predominantly as primary ferrite.

Weld cracking was not detected, either ultrasonically or metallographically, in any of the B/C welds. This observation is consistent with the principle that Type 304L stainless steel welds, which solidify as primary ferrite, are extremely resistant to weld hot cracking.

A/B welds. A macrograph of a transverse section from an A/B weld containing a centerline defect is shown in Fig. 4A. Note that the cracking is associated with a light-etching region, which is localized along the weld centerline and does not extend into the dark-etching regions of the weld. Solidification cracking in the A/B welds was always specific to the centerline region, usually midway between the top and bottom of the weld, and was always completely enveloped by the light-etching microstructure evident in Fig. 4A. Porosity was also observed in many of the cross sections of the A/B welds; this porosity was frequently associated with the light-etching microstructure.

The variation in etching characteristics in the A/B welds can be explained by the local change in ferrite content within the weld. At higher magnification in Fig. 5, it is evident that the light-etching centerline region is effectively fully austenitic. Solidification along the centerline in Fig. 5 appears to have occurred as primary austenite. The dark-etching microstructure surrounding the weld centerline has solidified as primary ferrite, as evidenced by the presence of retained delta ferrite along the cores of the solidification substructure. The shift in solidification behavior at the centerline is abrupt and appears to occur over a distance of approximately 20 microns. Note that the rapid transition in solidification behavior is accompanied by a change in the growth orientation of the solidification substructure.

The ferrite content of the A/B welds, as measured by the Magne Gage, was on the order of FN 2. This ferrite level agrees reasonably well with that predicted by the DeLong diagram in Fig. 3. The variation in solidification behavior within the weld cannot, however, be predicted by Fig. 3, if equal mixing of the A and B material is assumed to occur in the weld pool.

Microprobe Analysis

Microprobe analysis traverses were performed across the fully austenitic region at the weld centerline in an effort to determine if local changes in the weld metal composition were responsible for the shift in solidification behavior. The analysis region shown in Fig. 6 traversed a ferrite-free region near the tip of a centerline crack, which was bounded by regions of the fusion zone which solidi-

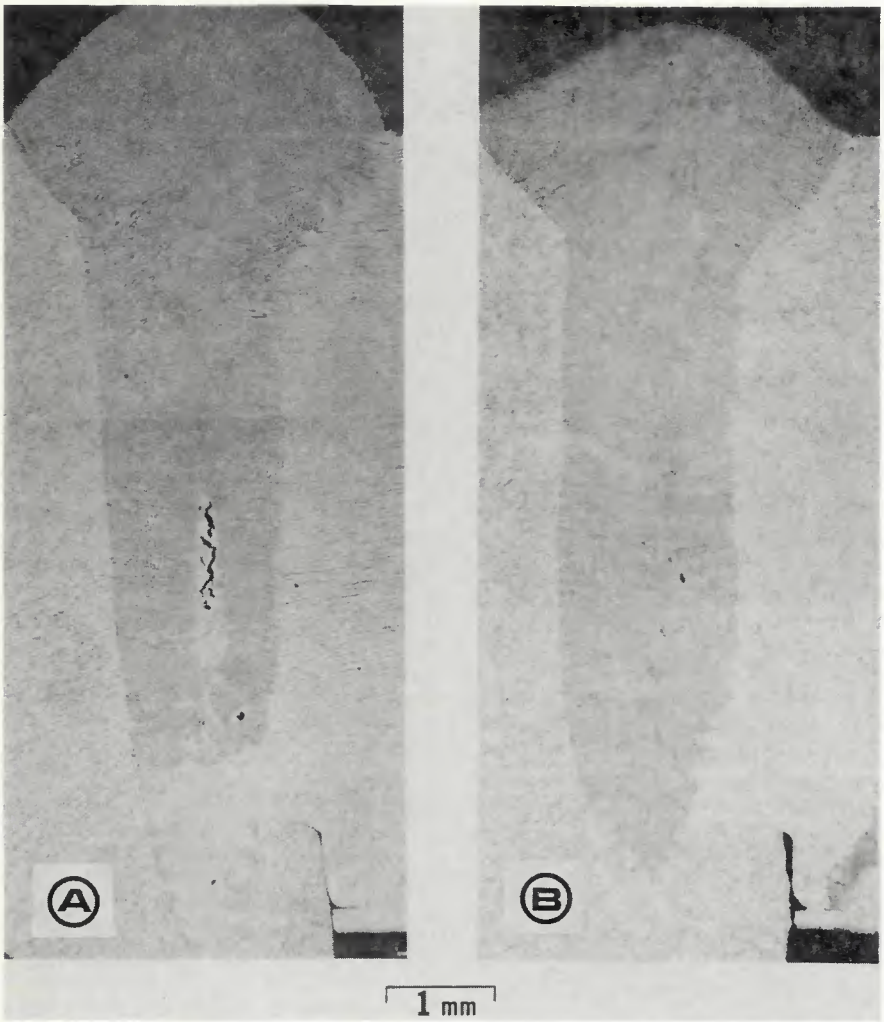

Fig. 4—Macrographs of weld transverse sections: A—A/B weld which exhibited centerline solidification cracking; B—B/C weld

fied as primary ferrite. Despite the shift in the primary phase of solidification, no corresponding shift in the concentration of the major alloying additions (Cr, Ni, Mn, Si) was associated with this transition.

The microprobe is relatively insensitive to carbon and nitrogen at the levels in which they are present in Type 304L stainless steel. Thus, quantitative concentration profiles for both of these powerful austenite stabilizing elements could not be obtained.

Discussion

The weld hot cracking observed in deep penetration EB welds between a low weld ferrite heat (material A) and medium weld ferrite heat (material B) of Type 304L stainless steel can be associated with a shift in solidification behavior along the weld centerline. No shift in solidification behavior or subsequent susceptibility to hot cracking was observed in identical welds made with two medium weld ferrite heats (materials B and C). The solidification behavior of 300-series stainless steel welds is primarily dependent on the weld metal composition (Refs. 5,17). Thus, the observed solidification anomaly in the A/B welds would be expected to be the result of a local variation in weld metal composition.

Centerline cracking in welds made at high velocity is often attributed to the macrosegregation of alloying and impurity elements along this narrow region during the final stages of solidification. Savage *et al.* (Ref. 32) have shown that an elongated, or tear-drop shaped, weld pool gives rise to a distinct centerline along which weld defects are prevalent. As the weld pool shape becomes more elliptical, the distinct centerline disappears and the propensity for weld defects generally decreases. Despite the utility of the macrosegregation theory, electron microprobe analysis was unable to detect any significant change in weld metal composition in the centerline region of the A/B welds—Fig. 6.

Similar shifts in solidification behavior along the weld centerline of autogenous GTA welds in Type 309 stainless steel have been reported by other investigators (Refs. 30,31). Microprobe analysis performed across the fully austenitic centerline region (Ref. 31) of the Type 309 stainless steel welds also failed to reveal any significant change in composition relative to the composition of the surrounding weld microstructure. The observation of centerline solidification transitions in the Type 309 stainless steel bead-on-plate welds was not complicated by the assumption of uniform mixing of two materials of different composition. Thus, it seems likely that the anomalous solidification behavior in the A/B electron beam welds is not due to nonhomogeneous mixing in the weld pool.

The microprobe data presented in Fig. 6 demonstrate that the segregation of major alloying elements is not responsible for the shift in solidification behavior along the centerline. The effect of carbon and nitrogen on the weld solidification behavior is more difficult to assess. Little information is available concerning the partitioning of these elements during weld solidification. Both carbon and nitrogen are extremely mobile in the material in the solidification temperature range; it is likely that any partitioning which occurs during solidification rapidly disappears through diffusion.

In a previous investigation (Ref. 33), the Auger microscope was used to detect the presence of both carbon and nitrogen on the centerline crack surface in similar welds. Carbon appeared to be present as an impurity, since it became undetectable as the surface layer (~20 nm)* was removed. Nitrogen was detectable in significant concentrations nearly 100 nm below the fracture surface. In addition, porosity was frequently associated with the fully austenitic region along the centerline. The combination of these two observations suggests that the segregation of nitrogen, a powerful austenite former, contributes to the solidification transition along the weld centerline in the A/B welds. The B/C welds have a lower average nitrogen content than the A/B welds and exhibit no change in solidification behavior or perceptible reduction in ferrite content along the centerline.

Suutala (Ref. 17) has observed a gradual shift in the solidification behavior of 300-series austenitic stainless steel welds and has attributed this shift to changes in the welding conditions. Nitrogen analyses of the weld metal, in which a shift from primary ferrite to primary austenite solidification had occurred, failed to detect any significant increase in nitrogen con-

**1 micron = 0.001 mm.*

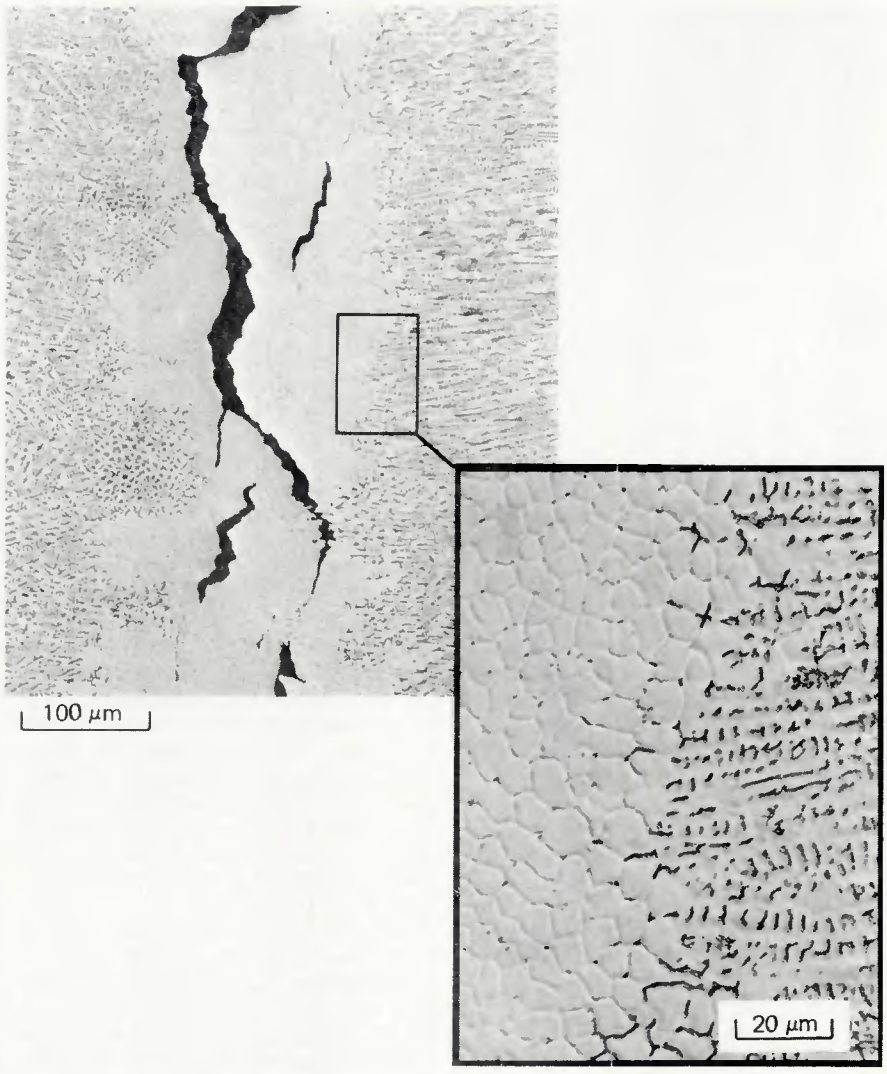

Fig. 5—Optical micrograph of the centerline region in an A/B weld. Note the rapid transition in both the primary mode of solidification and the solidification growth direction

tent. These results indicate that the local variation in the solidification behavior of the A/B welds may not be due exclusively to the segregation of nitrogen; instead, it may be controlled by a localized shift in solidification conditions at the weld centerline.

Effect of Solidification Conditions

An increase in the weld travel speed at equivalent current and voltage levels reduces the overall heat input of a weld while increasing the solidification growth rate along the solid-liquid interface at the trailing edge of the weld pool. The growth rate, R, during welding is related to the weld travel speed, V_w, by the expression

$$R \cong V_w \cos \theta$$

where θ represents the angle between the welding direction and the normal to the solid-liquid interface.

Using this expression, the growth rate along the trailing edge of the weld pool can be approximated. In high velocity GTA and electron beam welds, the shape of the molten pool approximates an elongated tear-drop. Assuming this weld pool geometry, the growth rate in a weld moving at 50 cm/min (20 ipm, approximately the speed at which the A/B and B/C electron beam welds were made) can be plotted as a function of position along the solid-liquid interface, as shown in Fig. 7.

At the leading edge of the solidification front (points A and B in Fig. 7), the growth rate is essentially zero. Slightly behind points A and B, the growth front rapidly approaches a steady state velocity as a consequence of the pool geometry. In the vicinity of the weld centerline, the angular differential between the solidification growth direction and the welding direction changes rapidly until, at some point along the centerline, the growth rate and the welding velocity are equivalent ($\theta = 0°$, $\cos 0° = 1$, therefore $R = V_w$).

Thus, for an elongated, or tear-drop shaped, weld pool, the solidification growth rate along the centerline can be significantly greater than the growth rate in the bulk of the weld. As the weld pool becomes more elliptical (at lower welding velocity), the angular differential between the growth direction and the welding direction changes gradually and a growth rate anomaly does not occur along the centerline.

Suutala (Ref. 17) has proposed that the critical ratio, Cr_{eq}:Ni_{eq}, which differentiates alloy compositions that solidify as ferrite from those that solidify as austenite, varies as a function of the solidification growth rate in the weld. This relationship is reproduced in Fig. 8. Note that, at growth rates below approximately 25 cm/min (10 ipm), the critical equivalency ratio is nearly constant. Above this growth rate, the critical ratio increases—that is, solidification as primary austenite becomes more favorable.

The results of Vitek and David (Ref. 29) have been incorporated in Fig. 8 in order to extrapolate the critical equivalency ratio to higher growth rates (dashed line in Fig. 8). They observed that laser welds in a Type 308 stainless steel weld pad made at 150 cm/min (~60 ipm) solidified as primary austenite despite a relatively high Cr_{eq}:Ni_{eq} ratio.

These results suggest that the critical equivalency ratio, which defines solidification behavior, changes extremely rapidly as the solidification growth rate increases above approximately 100 cm/min (40 ipm). Thus, as the welding velocity becomes extremely rapid, solidification as primary austenite occurs at much higher values of Cr_{eq}:Ni_{eq} than normally expected.

Solidification Behavior of A/B and B/C Welds

The range of solidification growth rates predicted for the A/B and B/C electron beam welds (Fig. 7) have been superimposed on the diagram in Fig. 8. The growth rate range of the B/C weld lies entirely above the line which separates primary ferrite from primary austenite solidification. As observed metallographically (Fig. 4), solidification within the entire B/C weld was as primary ferrite, including the region along the weld centerline where the growth rate is greatest (50 cm/min, *i.e.*, 19.7 ipm).

In contrast, the growth rate range in the A/B welds straddles the demarcation line. Thus, Fig. 8 predicts that the region of the weld which solidifies at the steady state growth rate (~10 cm/min or 3.9 ipm) will form ferrite as the primary phase of solidification; this will occur while the

rapid growth rate along the weld centerline favors solidification as primary austenite. The shift in solidification behavior predicted by Fig. 8 corroborates the microstructural evidence in Figs. 4A and 5.

Although local variations in the solidification growth rate may be sufficient to explain the change in solidification behavior, macrosegregation of austenite stabilizing elements along the weld centerline could also contribute to the observed behavior. For instance, the partitioning of nitrogen, a powerful austenite stabilizer, would lower the local equivalency ratio along the centerline and allow the transition to primary austenite solidification to occur at lower growth rates. It appears, however, that macrosegregation alone does not explain the shift in solidification behavior.

The combination of Figs. 7 and 8 can be used to predict the solidification behavior in other austenitic stainless steel welds where the weld metal composition, the welding velocity, and the approximate shape of the weld pool are known. In a true "tear-drop" geometry, only an extremely narrow region (actually a point) at the weld centerline would achieve a growth velocity approaching the welding speed. As a result, any shift in solidification behavior associated with an abrupt change in growth rate would be essentially undetectable.

In reality, the shape of a deep penetration electron beam weld pool is relatively complex and varies as a function of distance below the surface of the weld (Ref. 34). The upper portion of the welds shown in Fig. 4 exhibits the characteristic "nailhead." The weld pool in this region is much wider than elsewhere in the weld; thus, it is likely that the shape of the weld pool will vary correspondingly. Direct observation of the surface of an EB weld using high-speed cinematography suggests that the pool shape tends to approximate an ellipse more than a "tear-drop" (Ref. 34). Below the "nailhead," the weld pool width is reduced, and the shape approaches that of a truncated "tear-drop" (Refs. 34-36); here the degree of truncation is a function of the pool width, the depth below the surface, and the physical properties of the material.

The variation in the weld pool shape as a function of distance below the surface explains the difference in microstructure and solidification behavior in the A/B welds. In the "nailhead" region, the elliptical pool shape eliminates the distinct centerline and prevents the growth rate anomaly shown in Fig. 7. As the weld narrows below some critical dimension, the elliptical shape evolves into one that more closely approximates a truncated "tear-drop." The transition in shape gives rise to the distinct centerline which is

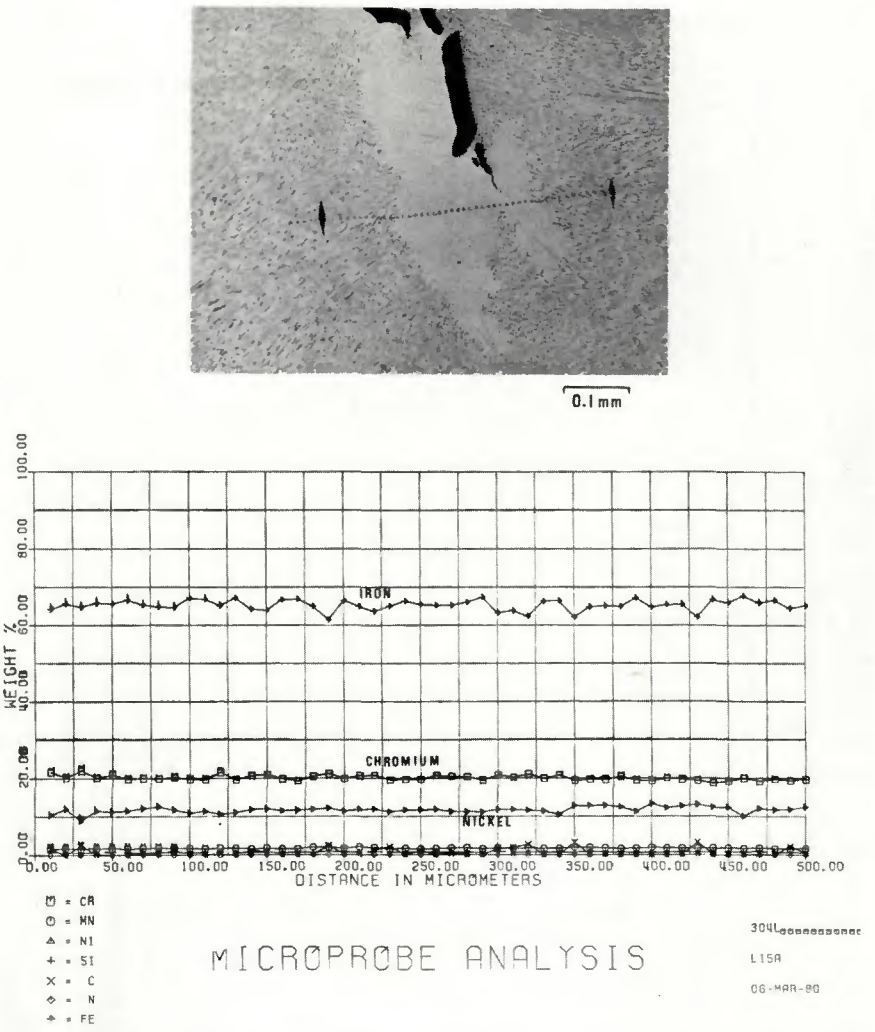

Fig. 6—Microprobe analysis traverse across a fully austenitic region at the centerline of an A/B weld

observed from approximately midway down in the weld to the weld root in Fig. 4. Within the A/B welds this centerline region solidifies as primary austenite and provides a preferential site for solidification cracking. The approximation of a truncated "tear-drop" for GTA welds made at high welding velocities also explains the observations of localized centerline primary austenite solidification and associated cracking reported in Type 309 stainless steel sheet stock (Refs. 30,31).

Solidification substructure size. Despite the abrupt change in solidification growth rate along the weld centerline in the A/B and B/C welds, the solidification substructure size—or primary dendrite arm spacing—in this region is comparable to that in the adjacent microstructure. The dendrite arm spacing is generally considered to be a function of both the temperature gradient, G, and the growth rate; this spacing obeys an inverse power law dependence on the product GR. Thus, a variation in the solidification growth rate uniquely controls the substructure size only when the gradient is constant.

Within a fusion weld, the temperature gradient at the solid-liquid interface varies significantly as a function of location along this interface. The gradient is the greatest at the edge of the weld where the solidification growth front initiates (points A and B in Fig. 7) and lowest along the centerline of the weld (Refs. 39,40). Sahm and Schubert (Ref. 35) have estimated that the temperature gradient along the edge of the weld can be two orders of magnitude greater than the gradient at the centerline.

The temperature gradient in the steady state growth region (Fig. 7) would vary between these two extremes and is probably a function of position along the interface. Since the growth rate along the solid-liquid interface changes in an opposite manner, the product GR should be roughly equivalent at all points along the weld interface except at the edge of the weld where the gradient is very steep. As a result, the substructure size in the bulk

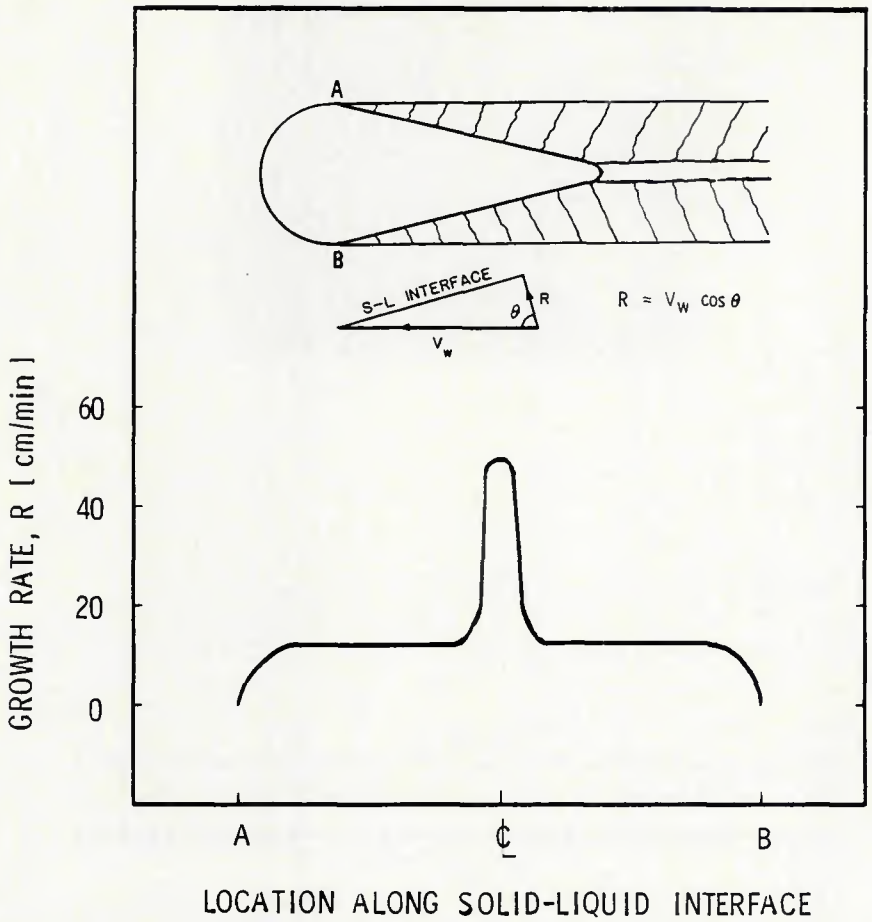

Fig. 7—Solidification growth rate as a function of location along the solid-liquid interface in a truncated, "tear-drop" shaped weld made at a welding velocity of 50 cm/min (20 ipm)

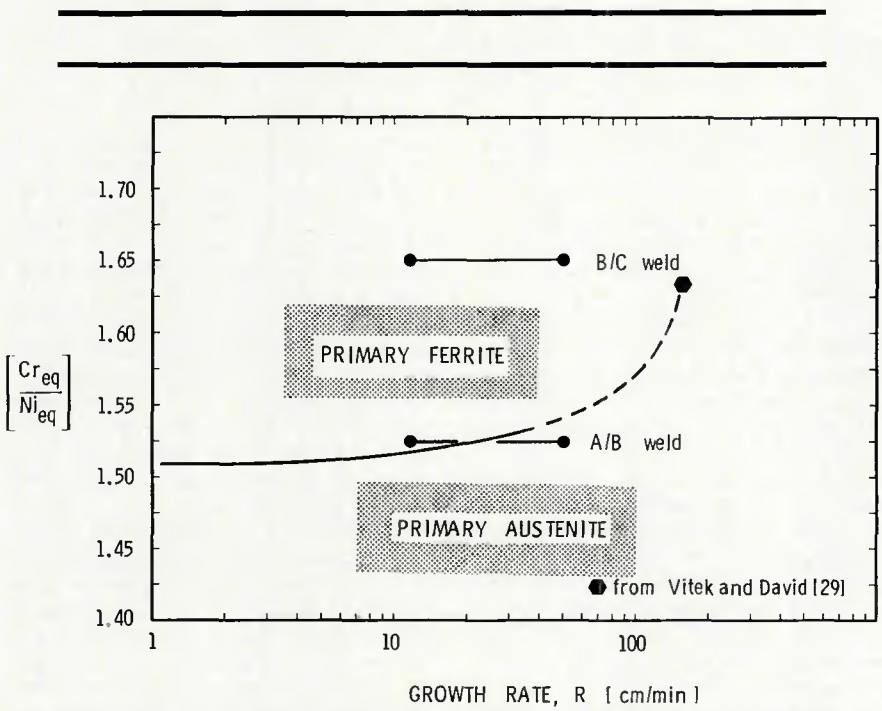

Fig. 8—Effect of composition (Cr_{eq}/Ni_{eq}) and solidification growth rate on the solidification behavior of 300-series stainless steels. The solid portion of the curve is taken from Suutala (Ref. 17). The range of solidification growth rates for the A/B and B/C welds is taken from Fig. 7, assuming a welding velocity of 50 cm/min (20 ipm)

of the weld should be relatively uniform.

Effect of "spiking" on solidification behavior. As noted previously, the B/C welds solidified as primary ferrite across the entire width of the weld. Close examination of Fig. 4B, however, reveals that a light-etching region is present in the root of this weld. The high magnification photomicrograph of this region (Fig. 9) reveals that the microstructure is nearly fully austenitic and exhibits an extremely fine solidification substructure. The origin of this microstructure is probably the result of a phenomenon known as "spiking" (Refs. 41,42), whereby an instability in the electron beam results in a momentary increase in weld penetration. As a result, a molten "spike" forms in the root of the weld and resolidifies extremely rapidly.

Reference to Fig. 8 indicates that the growth rate in this region must be greater than 150 cm/min (60 ipm) in order to produce the fully austenitic structure. Since the "spiking" phenomenon is essentially instantaneous, it is likely that the temperature gradient during solidification of the "spike" is high; thus, the GR product would be much larger than elsewhere in the weld. The presence of a fully austenitic microstructure within a weld, whose Cr_{eq}:Ni_{eq} ratio is relatively high, indicates the dominant effect of growth rate on the solidification behavior of austenitic stainless steels. In addition, this observation is in agreement with the results of Vitek and David (Ref. 29) and reinforces the dramatic increase in the critical equivalency ratio at growth rates above approximately 100 cm/min (39.4 ipm)—Fig. 8.

Relationship Between Solidification Behavior and Weld Hot Cracking

The solidification cracking observed in the A/B welds is the result of both a crack susceptible microstructure and a large inherent weld restraint associated with the weld geometry. In many practical applications, the weld penetration requirements and, hence, the restraint conditions are fixed. As a consequence, the solution to the weld cracking problem, such as in the A/B welds, often requires the selection of more crack resistant alloy composition.

When using the more conventional welding processes (GTAW, GMAW, SMAW, SAW), the DeLong diagram coupled with the Suutala relationship for the primary austenite/primary ferrite demarcation (Fig. 3) can be used successfully to select compositions which are resistant to hot cracking. However, when using high energy density welding processes (EBW, LW) or the more conventional processes at extreme welding speeds (>50 cm/min, *i.e.*, 19.7 ipm), the behavior predicted by

Fig. 3 may not be valid.

It is likely that the A/B combination would be readily weldable at welding velocities which did not produce an elongated weld pool. A corollary study (Ref. 43) has demonstrated that increasing the width of the A/B welds through both beam oscillation and reduced welding speed has essentially eliminated the fully austenitic region along the centerline. Unfortunately, redevelopment of the welding process/welding conditions is not always practical.

In general, the selection of an alternate material with a higher Cr_{eq}/Ni_{eq} value is the most appropriate means to ensure that welds are crack resistant. In this investigation, the substitution of material A with material C eliminated the weld cracking problem. It is interesting to note, however, that at even higher welding velocities (>150 cm/min, *i.e.*, 59 ipm), Fig. 8 predicts that a similar solidification transition may occur along the centerline of the B/C welds.

Although solidification as primary austenite is normally avoided by proper material selection, several investigators (Refs. 11,30,44,45) have demonstrated that crack-free, fully austenitic weldments can be produced if the material either contains extremely low impurity levels or is welded under low restraint conditions. For example, the bead-on-plate laser welds in Type 308 stainless steel studied by Vitek and David (Ref. 29) did not exhibit any cracking, despite solidifying as primary austenite. In general, the depth-to-width ratio of these welds was less than 1 and the total sulfur plus phosphorus content was less than 300 ppm. In contrast, Brooks *et al.* (Ref. 30) reported that bead-on-plate welds in Type 309 stainless steel exhibited cracking along a fully austenitic region at the weld centerline (welding velocity = 61 cm/min, *i.e.*, 24 ipm). These welds were highly restrained and contained from 200-1000 ppm sulfur plus phosphorus. In similar welds, where the impurity level was below 200 ppm, weld cracking was not observed, irrespective of solidification behavior.

In addition to the transition in solidification behavior which occurred along the centerline of the A/B welds, reference to Table 1 reveals that the average sulfur content of this material combination is greater than that of the B/C welds. In a previous report (Ref. 33), a significant amount of sulfur was detected both by the microprobe and Auger microscope in the vicinity of the solidification cracks and on the fracture surface.

The deleterious effect of sulfur with respect to weld hot cracking susceptibility in fully austenitic stainless steel welds is well known (Refs. 6,9-13). The threshold level of sulfur (and phosphorus) which promotes cracking is not well defined and is undoubtedly highly dependent on the level of weld restraint. Since the weld geometry used in this investigation produces significant restraint across the weld, the threshold impurity level, below which cracking does not occur during solidification as primary austenite, may be extremely low (<100 ppm).

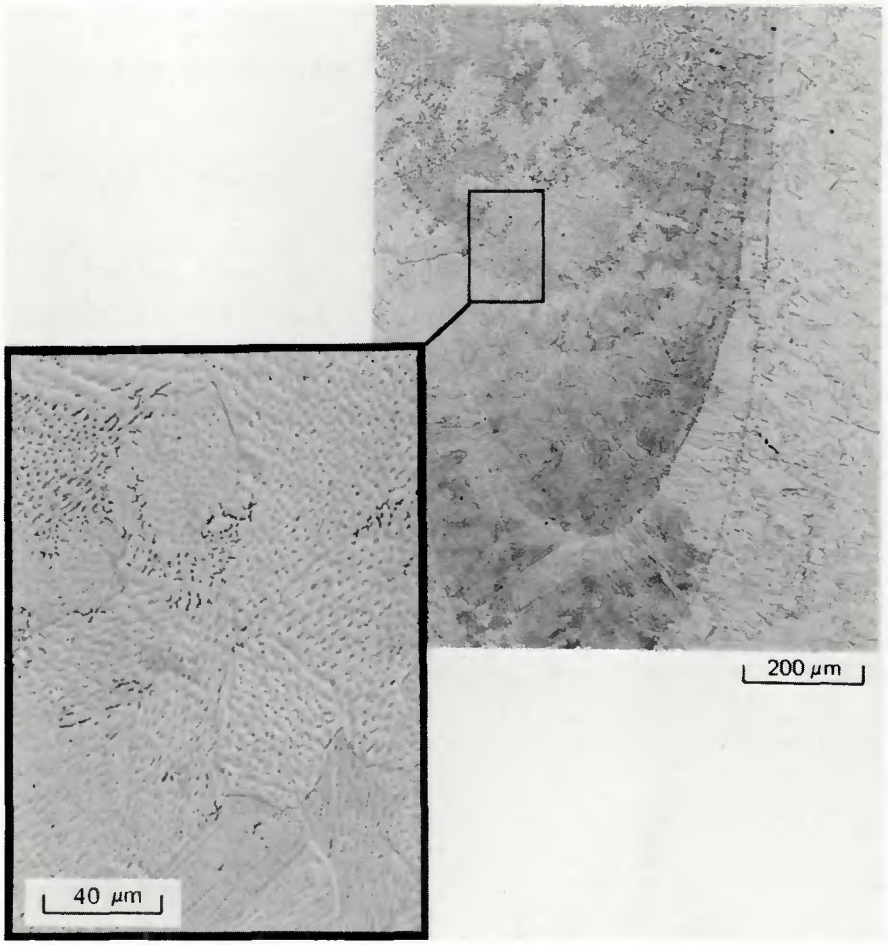

Fig. 9—Optical micrograph of the weld root region of a B/C weld. Rapid solidification due to electron beam "spiking" results in a nearly fully austenitic structure

Summary

Centerline solidification cracking in deep penetration electron beam welds between low and medium weld ferrite variants of Type 304L stainless steel is associated with a shift in solidification behavior. The DeLong and Suutala equivalency relationships predict that the weld metal ferrite content of this material combination should be in the range of FN 2-3 with solidification occurring as primary ferrite. Metallographic examination of these welds revealed that, while the bulk of the fusion zone solidifies as predicted, a narrow region along the weld centerline solidifies as primary austenite and contains no residual ferrite. Hot cracking is restricted to the fully austenitic region at the centerline. Similar welds between two medium ferrite variants of Type 304L stainless steel solidified as primary ferrite along the centerline and were not susceptible to cracking.

Microprobe analysis traverses performed across the fully austenitic centerline region failed to detect any segregation of austenite stabilizing elements which would give rise to the observed shift in solidification behavior. The shift from solidification as primary ferrite to primary austenite appears to be associated with an abrupt change in solidification conditions at the centerline. As a consequence of the rapid welding speed, the weld pool shape approximates a truncated "tear-drop"; the solidification growth rate at the centerline of this weld pool increases abruptly relative to that of the surrounding fusion zone.

In alloys, or alloy combinations, with a low Cr_{eq}/Ni_{eq} value (but which under normal welding conditions should solidify as primary ferrite), the large change in solidification growth rate promotes solidification as primary austenite. When the weld restraint is relatively severe such as in deep penetration electron beam

welds, the shift in solidification behavior can result in weld hot cracking.

Acknowledgment

This work was supported by the U.S. Department of Energy under contract No. DE-AC04-76DP00789. Special thanks are extended to the welding staff at General Electric Neutron Devices Division in St. Petersburg, Fla., for their cooperation during the course of this investigation.

References

1. Puzak, P. P., Apblett, W. R., and Pellini, W. S. 1956. Hot cracking of stainless weldments. *Welding Journal* 35(1):9-s to 17-s.

2. Borland, J. C. and Younger, R. N. 1960 (Jan.). Some aspects of cracking in welded Cr-Ni austenitic steels. *Brit. Weld. Jour.* pp. 22-59.

3. Hull, F. C. 1967. Effect of delta ferrite on the hot cracking of stainless steel. *Welding Journal* 46(9):399-s to 409-s.

4. Fredriks, H. and Vander Toorn, L. J. 1968 (April). Hot cracking in austenitic stainless steel weld deposits. *Brit. Weld. Jour.* pp. 178-182.

5. Masumoto, I., Tamaki, K., and Kutsuna, M. 1972. Hot cracking of austenitic stainless steel weld metal. *Trans. JWS* 41(11):1306-1341.

6. Arata, Y., Matsuda, F., and Saruwatari, S. 1974. Varestraint test for solidification crack susceptibility in weld metal of austenitic stainless steels. *Trans. JWRI* 3(1):79-88.

7. DeLong, W. T. 1974. Ferrite in austenitic stainless steel weld metal. *Welding Journal* 53(7):273-s to 286-s.

8. Lundin, C. D., DeLong, W. T., and Spond, D. F. 1975. Ferrite-fissuring relationship in austenitic stainless steel weld metals. *Welding Journal* 54(8):241-s to 246-s.

9. Brooks, J. A. and Lambert, F. J. 1978. The effects of phosphorus, sulfur, and ferrite content on weld cracking of type 309 stainless steel. *Welding Journal* 57(5):139-s to 143-s.

10. Kujanpaa, V., Suutala, N., Takalo, T., and Moisio, T. 1979. Correlation between solidification cracking and microstructure in austenitic and austenitic-ferritic stainless steel welds. *Weld. Res. Intl.* 9(2):55-70.

11. Lundin, C. D., Chou, C.-P. D., and Sullivan, C. J. 1980. Hot cracking resistance of austenitic stainless steel weldments. *Welding Journal* 59(8):226-s to 232-s.

12. Lippold, J. C. and Savage, W. F. 1982. Solidification of austenitic stainless steel weldments, part 3—the effect of solidification behavior on hot cracking susceptibility. *Welding Journal* 61(12):388-s to 396-s.

13. Brooks, J. A., Thompson, A. W., and Williams, J. C. 1984. A fundamental study of the beneficial effects of delta ferrite in reducing weld cracking. *Welding Journal* 63(3):71-s to 83-s.

14. Schaeffler, A. L. 1949. Constitution diagram of stainless steel weld metal. *Metal Progress* 56(5):680, 680b.

15. Hull, F. C. 1973. Delta ferrite and martensite formation in stainless steels. *Welding Journal* 52(5):193-s to 203-s.

16. DeLong, W. T., Ostrom, G., and Szumachowski, E. 1956. Measurement and calculation of ferrite in stainless steel weld metal. *Welding Journal* 35(11):526-s to 533-s.

17. Suutala, N. 1983. Effects of solidification conditions on the solidification mode in austenitic stainless steels. *Met. Trans.* 14A:191-197.

18. Hammar, O. and Svensson, U. 1979. Influence of steel composition on segregation and microstructure during solidification of austenitic stainless steel. *Solidification and Casting of Metals*, pp. 401-410. The Metals Society. London: 1979.

19. Arata, Y., Matsuda, F., and Katayama, S. 1976. Fundamental investigation of solidification behavior of fully austenitic and duplex microstructures and effect of ferrite on microsegregation. *Trans. JWRI* 5(2):35-51.

20. Takalo, T., Suutala, N., and Moisio, T. 1979. Austenitic solidification mode in austenitic stainless steel welds. *Met. Trans.* 10A:1173-1181.

21. Fredrikkson, H. 1972. Solidification sequence in an 18-8 stainless steel investigated by directional solidification. *Met. Trans.* 3(11):2989-2997.

22. Suutala, N., Takalo, T., and Moisio, T. 1979. Single phase ferritic solidification mode in austenitic-ferritic stainless steel welds. *Met. Trans.* 10A(8):1183-1190.

23. David, S. A., Goodwin, G. M., and Braski, D. N. 1979. Solidification behavior of austenitic stainless steel filler metals. *Welding Journal* 58(11):330-s to 336-s.

24. Lippold, J. C. and Savage, W. F. 1979. Solidification of austenitic stainless steel weldments, part 1—a proposed mechanism. *Welding Journal* 58(12):362-s to 374-s.

25. Brooks, J. A., Thompson, A. W., and Williams, J. C. 1982. Solidification and solid state transformations of austenitic stainless steel welds. *Trends in Welding Research in the United States*, pp. 331-357. Metals Park, Ohio: American Society for Metals.

26. Brooks, J. A., Williams, J. C., and Thompson, A. W. 1983. Microstructural origin of the skeletal ferrite morphology of austenitic stainless steel welds. *Met. Trans.* 14A:1271-1281.

27. Leone, G. L., and Kerr, H. W. 1982. The ferrite to austenite transformation in stainless steel. *Welding Journal* 61(1):13-s to 21-s.

28. Takalo, T., Suutala, N., and Moisio, T. 1976. Influence of ferrite content on its morphology in some austenitic weld metals. *Met. Trans.* 7A:1591-1592.

29. Vitek, J. M. and David, S. A. 1982. Microstructural analysis of austenitic stainless steel laser welds. *Trends in Welding Research in the United States*, pp. 243-258. Metals Park, Ohio: American Society for Metals.

30. Brooks, J. A., Thompson, A. W., and Williams, J. C. 1980. Weld cracking of austenitic stainless steels—effects of impurities and minor elements. *Proc. of TMS-AIME Symposium, Physical Metallurgy of Metal Joining*, St. Louis, October 1980, pp. 117-136.

31. Kou, S., and Le, Y. 1982. The effect of quenching on the solidification structure and transformation behavior of stainless steel welds. *Met. Trans.* 13A:1141-1152.

32. Savage, W. F., Lundin, C. D., and Chase T. F. 1968. Solidification of fusion welds in face-centered cubic metals. *Welding Journal* 48(11):522-s to 526-s.

33. Lippold, J. C. 1981. Weld cracking mechanisms in austenitic stainless steels. *Proc. of ASM Conference Trends in Welding Research in the United States*, New Orleans, November 1981, pp. 209-242.

34. Private communication, W. H. Giedt, July 1984.

35. Sahm, P. R. and Schubert, F. 1977. Solidification phenomenon and properties of cast and welded microstructures. *Proc. of Solidification and Castings of Metals*, Sheffield, England, pp. 389-400.

36. Wittke, K. 1975. *Schweisstechnic*, vol. 25, p. 290.

37. Davies, G. J. and Garland, J. G. 1975. *Int. Metall. Review* 20, p. 83.

38. Flemings, M. C. 1974. *Solidification processing*, p. 149. McGraw-Hill, Inc.

39. Rosenthal, D. 1941. Mathematical theory of heat distribution during welding and cutting. *Welding Journal* 20(5):220-s to 234-s.

40. Trivedi, R. and Srinivason, S. R. 1974. Temperature distribution around a moving cylindrical source. *Jour. of Heat Transfer, Trans. of the ASME* 96:427-428.

41. Armstrong, R. E. 1970. Control of spiking in partial penetration electron beam welds. *Welding Journal* 49(8):382-s to 388-s.

42. Schauer, D. A., and Giedt, W. H. 1978. Prediction of electron beam welding spiking tendency. *Welding Journal* 57(7):189-s to 195-s.

43. Unpublished research performed jointly by Sandia National Laboratories, Livermore, Calif., and General Electric Neutron Devices Division, St. Petersburg, Fla., 1982.

44. Arata, Y., Matsuda, F., and Katayama, S. 1977. Solidification crack susceptibility in weld metals of fully austenitic stainless steels. *Trans. JWRI* (6)1:105-116.

45. Honeycombe, J. and Gooch, T. G. 1972. Effect of manganese on cracking and corrosion behavior of fully austenitic steel weld metals. *Metal Construction and Brit. Weld. Jour.* 4(12):456-459.